

---

# SCALE-INVARIANT PROCESS REGRESSION

---

A PREPRINT

• **Matthias Wieler**

Bosch Center for Artificial Intelligence  
 Renningen, Germany  
 matthias.wieler@de.bosch.com

August 9, 2022

## ABSTRACT

Gaussian processes are the leading method for non-parametric regression on small to medium datasets. One main challenge is the choice of kernel and optimization of hyperparameters. We propose a novel regression method that does not require specification of a kernel, length scale, variance, nor prior mean. Its only hyperparameter is the assumed regularity (degree of differentiability) of the true function.

We achieve this with a novel non-Gaussian stochastic process that we construct from minimal assumptions of translation and scale invariance. The process can be thought of as a hierarchical Gaussian process model, where the hyperparameters have been incorporated into the process itself. To perform inference with this process we develop the required mathematical tools.

It turns out that for interpolation, the posterior is a  $t$ -process with a polyharmonic spline as mean. For regression, we state the exact posterior and find its mean (again a polyharmonic spline) and approximate variance with a sampling method. Experiments show a performance equal to that of Gaussian processes with optimized hyperparameters.

The most important insight is that it is possible to derive a working machine learning method by assuming nothing but regularity and scale- and translation invariance, without any other model assumptions.

**Keywords** Gaussian process regression · scale invariance · Wiener process · fractional Brownian motion ·  $t$ -process · polyharmonic spline

## 1 Introduction

**Gaussian process regression** Gaussian processes (GPs) are the leading method for non-parametric regression on small to medium datasets [Rasmussen and Williams, 2005]. Their main advantages over other regression methods are data efficiency (i.e. good performance even on few datapoints) and built-in uncertainty quantification (posterior distributions and credible intervals), which is based on the solid theoretical foundation of viewing regression as Bayesian inference in function space.

One main challenge in GP regression is finding the optimal hyperparameters: kernel shape, length scale, variance (amplitude in  $y$ -direction), and prior mean. The kernel shape is usually fixed by the ML practitioner (or chosen from a fixed small set via cross-validation), while the other hyperparameters are chosen by optimizing either the cross-validation error or the marginal likelihood.

This is both a computational and a conceptual challenge. On the computational side, hyperparameter optimization usually takes up the main share of the computational cost of training because it requires fitting the base model dozens or hundreds of times. On the conceptual side, the space of possible kernel shapes is infinite-dimensional, which can never be covered completely by hyperparameter optimization (HO), and the (pre-) selection of kernel is usually quite arbitrary<sup>1</sup>. Also, we should mention that HO by itself is quite contrary to the Bayesian approach; in principle we would

---

<sup>1</sup>most applications do not provide prior information about which kernel is appropriate

like to perform Bayesian integration over all hyperparameters (see e.g. Flaxman et al. [2015]), which is even more expensive and rarely done in practice.

**Self-similarity and scale invariance** The Wiener process (a special type of Gaussian process) is well-known to be self-similar, which means that if  $W(x)$  is a Wiener process, then  $W(sx)/\sqrt{s}$  is also a Wiener process for any  $s$ . Self-similarity also holds for the (multiple-times) integrated Wiener process, fractional Brownian motion, and multi-dimensional versions of these processes. In the following we will use the name *Wiener-type* processes for all isotropic Gaussian processes that are self-similar  $W(x) \sim W(sx)/s^\eta$  with some exponent  $\eta$ .

Self-similarity is sometimes called “scale invariance” because  $s$  is a scale parameter. We want to stress, however, that Wiener-type processes are invariant only under a *simultaneous* change of  $x$ - and  $y$ -scale, and *not* under independent changes of either  $x$ - or  $y$ -scale. Therefore, it is more appropriate to say that Wiener-type processes exhibit a *coupling* of  $x$ - and  $y$ -scales than to say they were “scale invariant”. We stress this because the process we will propose is scale invariant in both  $x$  and  $y$  independently of each other.

**Splines** There is a close relation between the Wiener-type processes and splines. Concretely, maximum posterior estimation with a Wiener-type process prior is equivalent to minimizing a differential operator norm and results in natural splines in a single dimension and polyharmonic splines in multiple dimensions. This relation has been established by Kimeldorf and Wahba [1970], Duchon [1977], and Wahba [1990] and is well-known in statistics. However, these types of GPs are usually only applied in one or few ( $\leq 3$ ) dimensions, and the treatment is mostly limited to the maximum posterior estimate. The corresponding Gaussian processes are usually only mentioned in passing (often by the name “Kriging”) and the posterior distribution provided by the GP is rarely utilized (see e.g. Wendland [2004] and Fasshauer [2007]). There is in general little overlap between the spline literature and the literature on GPs in machine learning.

**Wiener-type processes in ML** The connection between Wiener-type processes and splines is known in machine learning [Rasmussen and Williams, 2005, chap. 6.3] and often used for demonstration purposes, but for real applications Wiener-type processes do not play a role. We believe this is due to three reasons: (i) missing wide-spread knowledge about the multidimensional Wiener-type processes, (ii) non-stationarity of Wiener-type processes, and (iii) missing appreciation of the importance and usefulness of scale invariance.

Concerning (i), we are not aware of a good reference for Wiener-type processes in general. Some helpful sources are [Kroese and Botev, 2015] on the fractional Brownian field, and [Encyclopedia, 2020] on the “Lévy  $D$ -parameter Brownian motion” (which is a different name for the Brownian field). This should not be confused with the non-isotropic “fractional Wiener sheet” or “ $D$ -parameter Wiener field”.

Concerning (ii), Wiener-type processes are not translation invariant, but fixed at the origin  $W(x=0) = 0$ . This is in contrast to most ML applications, which do not have a distinguished point in feature space, so that stationary GPs are a more obvious choice. In principle it is of course possible to use a hierarchical approach with a shift parameter  $x_0$  that has a uniform prior. This would render the Wiener-like processes stationary, but to our knowledge nobody has made the effort to pursue such an approach.

Concerning (iii), Rasmussen and Williams [2005, p. 137] argue that the scale invariance (i.e. self-similarity) of the Wiener-type processes is not a desirable feature, because applications *do* have a distinguished scale; and instead they favor a hierarchical approach that models this scale explicitly. In fact our proposed method is similar to such a hierarchical model, and our posterior *does* have a distinguished scale; but as this paper will show, we can avoid the complexity of the hierarchical model by starting off from the assumption of scale invariance.

**Our approach** The path we pursue in this paper is to exploit invariance principles to the fullest possible extent. We first generalize the well-known scale invariant (hyperbolic) prior to a scale invariant stochastic process. By doing this we leave the ground of Gaussian processes and of reproducing kernel Hilbert spaces.

Then we impose a power-law spectrum which naturally leads us to the same theory that connects GPs with splines. We mostly work in frequency space (in part similar to Kent and Mardia [1994]), which provides a simplified and generalized perspective on the known theory. Especially, our approach extends naturally to fractional exponents, which connects the theory to fractional Brownian fields and fractional derivatives (of the Riesz type).

To avoid confusion, we must mention in this context that there is a long circulated error in polyharmonic spline theory. The radial basis functions containing the logarithm  $r^k \log r$  (with even  $k$ ) yield interpolants that have infinite norm<sup>2</sup> instead of minimizing the norm. In fact, the case of even  $k$  is degenerate and can be treated only as the limit of fractional  $k$ . This issue will require a more thorough treatment elsewhere.

---

<sup>2</sup>over  $\mathbb{R}^D$

**Overview of paper** In Section 2 we construct the novel scale invariant process. Section 3 derives the interpolation solution, which is to a large part a simplified and generalized version of known theory. In Section 4 we present a basic method to perform regression with the scale invariant process. Some results are shown in Section 5, and Section 6 discusses the relevance and impact of the work.

## 2 The scale invariant process (SIP)

### 2.1 Hierarchical GP model

To give a first idea of the scale invariant process, we state a hierarchical GP model in a single input dimension that is closely related to the SI process.

$$f(x) = u_y + h_y \cdot W^{(\frac{1}{2}-\eta)}(u_x + h_x x) \quad (1)$$

$W^{(-l)}$  is the  $l$ -times integrated Wiener process. The expression of the exponent (with  $\eta$  being a positive half-integer) is chosen for consistency with the following. The hyperparameters  $u_x, u_y, h_x, h_y$  are independent random variables distributed uniformly  $p(u_{x,y}) \propto 1$  for  $u_{x,y} \in \mathbb{R}$ , or hyperbolically  $p(h_{x,y}) \propto 1/h$  for  $h_{x,y} \in \mathbb{R}_+$ , resp. The hyperparameters make the model translation and scale invariant in both input and output ( $x$ - and  $y$ -direction), independently of each other.

The scale-invariant process that we develop in the following will turn out to be similar to (1), but with the advantages of (i) being derived from minimal assumptions about invariance and (ii) having the hyperparameters “incorporated into the stochastic process itself”.

### 2.2 Overview of the construction

The two main steps of the following construction are illustrated in Figure 2. The probability distribution (or rather: law of the stochastic process)  $p$  is defined over functions  $f$  over the input  $x$ . Roughly speaking, the upper part of Figure 2 describes the  $y$ -dependence of the process, while the lower part describes the  $x$ -dependence. The concept of scale invariance must be implemented in different ways for the two parts.

We start with scale invariant distributions in finite dimensions, generalize this to a scale invariant stochastic process, and then impose a scale invariant (power-law) spectrum on the process.

### 2.3 Scale invariance in $\nu$ dimensions

Since the domain of our distributions are function values  $f_i = f(x_i)$ , we use the somewhat unusual symbol  $\mathbf{f}$  for the variable vector.

A distribution in  $\nu$  dimensions is scale invariant iff it satisfies the following differential and resulting functional equation.

$$p(\mathbf{f}) d\mathbf{f} = p(s\mathbf{f}) s^\nu d\mathbf{f} \quad (2)$$

$$p(s\mathbf{f}) = \frac{1}{s^\nu} p(\mathbf{f}) \quad (3)$$

The functional equation (3) determines the radial behavior of  $p(\mathbf{f})$ , but leaves the tangential behavior unspecified. The simplest possible choice would be spherically symmetric, but we need to take the “second-simplest possible” choice of ellipsoidal symmetry in order to allow correlations between different  $x$  (see Section 2.5). Thus we have

$$p_{\text{SI}}(\mathbf{f}) = \frac{1}{\|\mathbf{f}\|_a^\nu} \quad (4)$$

$$\|\mathbf{f}\|_a^2 = \sum_{i=1}^{\nu} \left( \frac{f_i}{a_i} \right)^2 \quad (5)$$

The coefficients  $a_i \in \mathbb{R}_+$  can be interpreted as amplitudes and will be specified below.

Note that the distribution (4) is improper. Its integral diverges both for  $\|\mathbf{f}\| \rightarrow 0$  and  $\|\mathbf{f}\| \rightarrow \infty$

$$\int_{\|\mathbf{f}\| < c} p_{\text{SI}}(\mathbf{f}) d\mathbf{f} = \infty \quad \int_{\|\mathbf{f}\| > c} p_{\text{SI}}(\mathbf{f}) d\mathbf{f} = \infty \quad \forall c > 0 \quad (6)$$

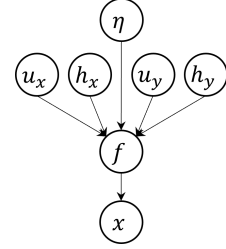


Figure 1: Hierarchical GP model

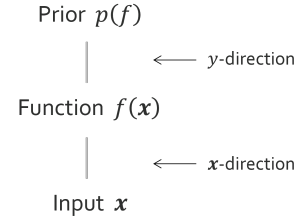


Figure 2: Objects of a stochastic process

## 2.4 Scale invariant process

The usual way to deal with the “infinite-dimensional distribution” of a stochastic process is to consider marginal distributions of finitely many function values  $\mathbf{f} = [f(\mathbf{x}_1), \dots, f(\mathbf{x}_\nu)]$ . These marginals obviously satisfy the following consistency relation

$$p(\mathbf{f}_1) = \int p(\mathbf{f}_1, \mathbf{f}_2) d\mathbf{f}_2 \quad \text{for all partitions } \mathbf{f}_1 \cup \mathbf{f}_2 = \mathbf{f}, \quad \mathbf{f}_1 \cap \mathbf{f}_2 = \emptyset \quad (7)$$

Conversely, the Daniell–Kolmogorov theorem states that any collection of finite-dimensional distributions that satisfy (7) defines a valid stochastic process. It is quite straightforward to show that (7) holds for the scale invariant distributions (4) for any choice of  $a_i$  (see Appendix 7.1). In this sense, we can interpret (4) as defining a scale invariant process. We call this general form a  $y$ -scale invariant process, since the  $\mathbf{x}$  dependence has not yet been specified.

Note that the consistency criterion (7) does not imply any constraint the amplitudes  $a(\mathbf{x})$ . This is in contrast to Gaussian processes, where (7) requires the covariance function to be positive semi-definite.

It is important to point out that the scale invariant process is improper, just like the scale invariant distributions. We do not know of any other improper stochastic process, and we do not know theory about improper processes. However, we did not encounter problems with the scale invariant process as constructed above. In general, Bayesians have had good experience with improper distributions, and we believe that this will extend to improper stochastic processes.

## 2.5 Spectrum

Now we specify the amplitudes  $a_i$  in (5). To achieve translation invariance in  $\mathbf{x}$  (lower part of Fig. 2), it is necessary to specify the amplitudes in frequency space  $a(\mathbf{k})$  instead of position space. Scale invariance requires that no scale (i.e. no frequency  $\mathbf{k}$ ) is distinguished from any other, which is only the case for power-law spectra.

$$a_\eta(\mathbf{k}) = \frac{1}{\|\mathbf{k}\|_\alpha^{\eta + \frac{D}{2}}} \quad (8)$$

$$\|\mathbf{k}\|_r^2 = \sum_{d=1}^D \left( \frac{k_d}{r_d} \right)^2 \quad (9)$$

The form of the exponent in (8) has been chosen such that  $\eta$  describes the regularity of the resulting process’s sample paths (see following paragraph).  $D$  is the number of dimensions of input space (length of vectors  $\mathbf{x}$  and  $\mathbf{k}$ ), and the parameters  $r_d$  describe the scaling of different input dimensions. For the current work we assume isotropic input space, i.e.  $r_d = 1$  for all  $d$ .

## 2.6 Regularity

The scale invariant spectrum is sketched in Fig. 3. The regularity of the process’s sample functions  $f(\mathbf{x})$  is determined by the asymptotic behavior of  $a(\mathbf{k})$  for  $\|\mathbf{k}\| \rightarrow \infty$ . We will show in Appendix 7.2 that for any spectrum that approaches (8) for  $\|\mathbf{k}\| \rightarrow \infty$ , the corresponding sample paths  $f(\mathbf{x})$  are  $C$  times differentiable, with the highest existing derivative being  $\alpha$ -Hölder continuous for all  $\alpha < H$ , where  $C$  and  $H$  are given by:

$$\text{degree of differentiability:} \quad C = \lfloor \eta \rfloor \quad (10)$$

$$\text{Hölder/Hurst exponent:} \quad H = \eta - C \quad (11)$$

Here and throughout this paper,  $\eta$  is constrained to being a positive non-integer, i.e.  $\eta \in (\mathbb{R}_+ \setminus \mathbb{N}_+)$ .

The Hölder exponent (usually called “Hurst exponent” in the context of fractional Brownian motion) is a real number in the open interval  $(0, 1)$  that generalizes the discrete degree of differentiability to a continuous notion of regularity. For the Wiener process (and integrals thereof) we have  $H = 1/2$  which corresponds to independent increments. Hölder/Hurst exponents larger/smaller than  $1/2$  describe positively/negatively correlated increments [Encyclopedia, 2016]. The transition between different degrees of differentiability happens at integer  $\eta$ , i.e. Hölder/Hurst exponent  $H = 0, 1$ . These cases are degenerate and we therefore exclude them throughout this paper.

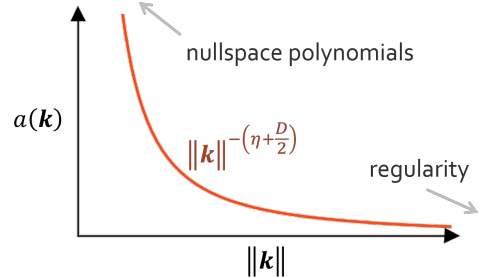


Figure 3: Spectrum of scale-invariant process

For Gaussian processes, several special cases of (10, 11) have been known for a long time. For instance, Flandrin [1989] gives the result for fractional Brownian motion ( $D = 1$ ,  $\eta \in (0, 1)$ ), and Molchan [1967] gives the result for Lévy  $D$ -parameter Brownian motion ( $\eta = 1/2$ ). As we show in Appendix 7.2, this result also holds for the scale invariant process and for all  $(D, \eta)$ .

Note that the exponent in (8) also appears in the power spectrum of the Matérn kernel (length-scale denoted by  $l$ ):

$$S_{\text{Matérn}}(\mathbf{k}) = a_{\text{Matérn}}^2(\mathbf{k}) \propto \left( \frac{\eta}{2\pi^2 l^2 + \|\mathbf{k}\|^2} \right)^{-(\eta + \frac{D}{2})} \quad (12)$$

$$a_{\text{Matérn}}(\mathbf{k}) \xrightarrow{\|\mathbf{k}\| \rightarrow \infty} \|\mathbf{k}\|^{-(\eta + \frac{D}{2})} \quad (13)$$

The regularity parameter  $\eta$  is usually denoted  $\nu$  in the context of Matérn kernels and chosen as a half-integer  $1/2$ ,  $3/2$ , or  $5/2$ , because this leads to a simple representation of the kernel in position space. The corresponding sample paths<sup>3</sup> are well-known to be continuously differentiable 0, 1, and 2 times, resp., and we can now add: with standard Hölder/Hurst exponent  $H = 1/2$ .

## 2.7 Nullspace

The spectrum (8) has a pole at  $\mathbf{k} = 0$ . To study the consequences of this pole we consider the continuous version of the norm (5)

$$|f|_\eta^2 = \int \left( \frac{\hat{f}(\mathbf{k})}{a_\eta(\mathbf{k})} \right)^2 d\mathbf{k} = \int \left( \Delta^{\frac{\eta}{2} + \frac{D}{4}} f(\mathbf{x}) \right)^2 d\mathbf{x} \quad (14)$$

We have added the position space representation with the Laplace operator  $\Delta$ , because this representation has been used much more often in the literature, e.g. in Rasmussen and Williams [2005, chap. 6.2, 6.3], especially for the 1D case, where the integrand reduces to  $(f^{(\eta+D/2)}(x))^2$ .

Th  $\eta$ -norm (14) vanishes for all polynomials up to degree  $\lfloor \eta \rfloor$ , or more exactly:

$$|\mathbf{x}^\nu|_\eta = \left| \prod_{d=1}^D x_d^{\nu_d} \right|_\eta = \begin{cases} 0 & |\nu| < \eta \\ \infty & |\nu| > \eta \end{cases} \quad (15)$$

where  $\nu = [\nu_1, \dots, \nu_D]$  is a multi-index with absolute value  $|\nu| = \sum_d \nu_d$ . This result can be found e.g. in [Wahba, 1990], and we rederive it in Appendix 7.3. The number of vanishing monomials, i.e. the dimension of the  $\eta$ -norm's nullspace can be expressed by the binomial coefficient

$$N_0 = \binom{\lfloor \eta \rfloor + D}{\lfloor \eta \rfloor} \quad \text{for positive non-integer } \eta \quad (16)$$

## 3 Interpolation

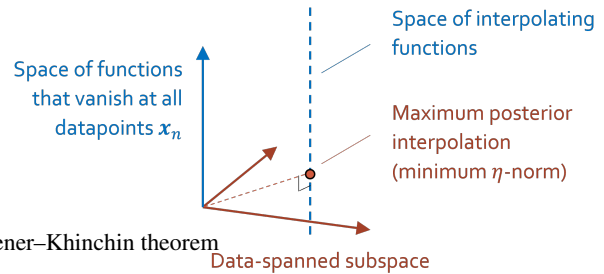
In this section, we condition the scale invariant process on  $N$  datapoints  $((\mathbf{x}_1, y_1), \dots, (\mathbf{x}_N, y_N)) = (X, \mathbf{y})$ . The result is a  $t$ -process with  $N - N_0$  degrees of freedom whose mean is the polyharmonic interpolation spline of the data with radial basis function  $g(\mathbf{x}) = \|\mathbf{x}\|^{2\eta}$  (positive non-integer  $\eta$ ). To derive this result, we first construct the function space that is spanned by the datapoints, then we formulate the maximum posterior solution, and finally we determine the pointwise conditional distribution.

### 3.1 Data-spanned subspace

We consider the function space  $\mathcal{F}_\eta$  that is defined by the inner product

$$\langle f, g \rangle_\eta = \int \frac{\hat{f}(\mathbf{k}) \hat{g}(\mathbf{k})}{a_\eta^2(\mathbf{k})} d\mathbf{k} \quad (17)$$

which induces the  $\eta$ -norm (14). The important property of this space is that the scale invariant process is isotropic in  $\mathcal{F}_\eta$ .



<sup>3</sup>which have the same spectrum as the kernel as per the Wiener-Khinchin theorem

Figure 4: Data-spanned subspace within function space  $\mathcal{F}_\eta$

We should point out that due to the nullspace of the  $\eta$ -norm,  $\mathcal{F}_\eta$  is *not* a Hilbert space and in particular not an RKHS<sup>4</sup>. But as we will see in the following, we still have all required tools at hand to solve the regression problem.

Our first goal is to find the subspace of  $\mathcal{F}_\eta$  that is “spanned by the data”, i.e. that is  $\eta$ -orthogonal to all functions that vanish at the datapoints  $X$ . As illustrated in Fig. 4, this subspace (denoted by  $\mathcal{S}_X$ ) is  $\eta$ -orthogonal to the space of all interpolating functions, and hence contains the interpolating function with minimum  $\eta$ -norm, which is the maximum posterior solution of interpolation.

To construct  $\mathcal{S}_X$  we need the Green’s functions  $g_\xi$  of the operator  $O[f] = \hat{f}(\mathbf{k})/a_\eta^2(\mathbf{k})$ , which by definition satisfy  $O[g_\xi] = \delta_\xi$ . The situation is clearest when giving both the position space and the frequency space representations:

$$O[f(\mathbf{x})] = \Delta^{\eta + \frac{D}{2}} f(\mathbf{x}) \quad O[\hat{f}(\mathbf{k})] = \frac{\hat{f}(\mathbf{k})}{a_\eta^2(\mathbf{k})} = \hat{f}(\mathbf{k}) \cdot \|\mathbf{k}\|^{2\eta + D} \quad (18)$$

$$g_\xi(\mathbf{x}) = \frac{1}{\tilde{C}} \|\mathbf{x} - \xi\|^{2\eta} \quad \hat{g}_\xi(\mathbf{k}) = \frac{\exp(2\pi i \mathbf{k} \xi)}{\|\mathbf{k}\|^{2\eta + D}} \quad (19)$$

$$O[g_\xi] = \delta_\xi \quad O[\hat{g}_\xi(\mathbf{k})] = \exp(2\pi i \mathbf{k} \xi) \quad (20)$$

In (18),  $\Delta$  is the Laplace operator. The constant  $\tilde{C}$  in (19) is not important at this point. The Green’s function in position space is most easily seen from the Fourier pair of generalized functions established by Gelfand and Shilov [1964]

$$\|\mathbf{x}\|^\gamma \longleftrightarrow \frac{\tilde{C}}{\|\mathbf{k}\|^{\gamma + D}} \quad \begin{array}{l} \gamma \in \mathbb{R} \\ \gamma \neq 2, 4, 6, \dots \\ -(\gamma + D) \neq 2, 4, 6, \dots \end{array} \quad (21)$$

In our function space  $\mathcal{F}_\eta$ , the Green’s functions are  $\eta$ -biorthogonal to the delta functions

$$\langle \delta_{\xi_1}, g_{\xi_2} \rangle_\eta = \langle \delta_{\xi_1}, \delta_{\xi_2} \rangle = \delta(\xi_1 - \xi_2) \quad (22)$$

and hence the data-centered Green’s functions  $g_{\mathbf{x}_n}$  are  $\eta$ -orthogonal to the functions vanishing at the datapoints. Unfortunately, however,  $g_{\mathbf{x}_n}$  are not mutually  $\eta$ -orthogonal, and worse, they have infinite  $\eta$ -norm, so they don’t belong to  $\mathcal{F}_\eta$ . Therefore, we cannot use them directly as basis functions for the sought subspace  $\mathcal{S}_X$ .

To solve the problem of infinite norm  $|g_{\mathbf{x}_n}|_\eta = \infty$ , we point out that it can be attributed to the fact that the biorthogonals “grow too fast” as  $\|\mathbf{x}\| \rightarrow \infty$ . Inserting (19) into (17), one can see quite directly that only functions with growth-rate smaller than  $\|\mathbf{x}\|^\eta$  have finite  $\eta$ -norm. Fortunately, it is possible to construct linear combinations of Green’s functions that satisfy this maximal growth-rate and are hence finite in  $\mathcal{F}_\eta$ . The result, which will be shown in Appendix 7.4 is that  $\mathcal{S}_X$  consists of all linear combinations of  $g_{\mathbf{x}_n}$  whose coefficients  $\mathbf{a}$  satisfy the growth-rate constraints(24).

$$f_X(\mathbf{x}) = \sum_{n=1}^N a_n g_{\mathbf{x}_n}(\mathbf{x}) \quad (23)$$

$$M\mathbf{a} = 0 \quad \Longleftrightarrow \quad |f_X|_\eta < \infty \quad (24)$$

$$M_{\nu n} = \mathbf{x}_n^\nu = \prod_{d=1}^D (\mathbf{x}_n)_d^{\nu_d} \quad |\nu| < \eta \quad (25)$$

The coefficients  $\mathbf{a}$  should not be confused with the amplitude  $a(\mathbf{k})$ . The dimension of  $\mathcal{S}_X$  is  $N - N_0$ , see (16).

Note that the above geometric argument in frequency space corresponds to the Euler-Lagrange equation in position space.

### 3.2 Maximum posterior interpolation

It might be surprising that  $N$  datapoints span a subspace of only  $N - N_0$  dimensions. The reason is that these  $N_0$  dimensions are hidden in the nullspace of  $\mathcal{F}_\eta$  and of  $\mathcal{S}_X$ . The complete space needed for interpolation is the Cartesian product  $\mathcal{S}_X^* = \mathcal{S}_X \times \mathcal{N}$ , where  $\mathcal{N}$  contains all nullspace polynomials.

<sup>4</sup>reproducing kernel Hilbert space

In  $\mathcal{S}_X^*$  we have  $N + N_0$  degrees of freedom (coefficients of the Green’s functions and the monomials), and  $N + N_0$  constraints (interpolation constraints and growth-rate constraints). Together, this yields the following linear system that describes the maximum posterior solution of interpolation  $f_{X,y}$ :

$$G_{nm} = g_{x_m}(\mathbf{x}_n) = \|\mathbf{x}_n - \mathbf{x}_m\|^{2\eta} \quad (26)$$

$$\begin{pmatrix} G & M^T \\ M & 0 \end{pmatrix} \begin{pmatrix} \mathbf{a} \\ \mathbf{c} \end{pmatrix} = \begin{pmatrix} \mathbf{y} \\ 0 \end{pmatrix} \quad (27)$$

$$f_{X,y}(\mathbf{x}) = \sum_{n=1}^N a_n g_{x_n}(\mathbf{x}) + \sum_{|\nu| < \lfloor \eta \rfloor} c_\nu \mathbf{x}^\nu \quad (28)$$

### 3.3 Relation to polyharmonic splines

The result (26–28) is known as polyharmonic<sup>5</sup> spline interpolation, and is textbook knowledge in the corresponding field (see e.g. Wendland [2004] or Fasshauer [2007]).

Our derivation adds to the existing treatments in that it clarifies the range of  $\eta$  for which the result is valid. Polyharmonic splines are usually defined for positive integer and half-integer  $\eta$  (i.e. for positive integers of the typically used parameter  $k = 2\eta$ ). Our derivation, on the contrary, is valid for all positive (fractional)  $\eta$  *except* for the integers. The problem with integer  $\eta$  is that their Green’s functions include the logarithm ( $\|\mathbf{x}\|^{2\eta} \log \|\mathbf{x}\|$ ), and as a consequence, the “linear combination trick” to obtain finite  $\eta$ -norm does not work anymore.

Numerical experiments show that as  $\eta$  approaches an integer, the coefficients  $[\mathbf{a}, \mathbf{c}]$  in (27) diverge, but the interpolant (28) approaches a finite limit. We believe that this limit is the correct solution for integer  $\eta$ , but that requires a more thorough treatment elsewhere.

### 3.4 Posterior process

Now we seek the stochastic process that results from applying the interpolation constraints on the scale invariant process. We know<sup>6</sup> that the polyharmonic spline (28) is the mean of this process, but the “distribution” over all possible interpolation functions (i.e. over the dashed line in Fig. 4) remains to be determined.

In the following, we denote vectors in the data-spanned subspace  $\mathcal{S}_X$  by  $\mathbf{h}$ . The relation between the components of  $\mathbf{h}$  and the biorthogonal and polynomial coefficients  $[\mathbf{a}, \mathbf{c}]$  will be deferred to Section 4.1.

To determine the shape of the posterior process, we only need to observe that conditionals of the SI distribution are Student  $t$ -distributions. More precisely, let  $\mathbf{h} = [\mathbf{h}_h, \mathbf{h}_t]$  be the combination of two vectors of length  $N_h, N_t$ , resp., with combined length  $N_{ht} = N_h + N_t$ , and let  $\mathbf{h}$  be distributed according to the isotropic SI distribution. Then the conditional distribution  $p(\mathbf{h}_t | \mathbf{h}_h)$  is a multivariate  $t$ -distribution with  $N_h$  degrees of freedom (unless  $\|\mathbf{h}_h\| = 0$ ).

$$p(\mathbf{h}) = \frac{1}{\|\mathbf{h}\|^{N_{ht}}} \quad (29)$$

$$p(\mathbf{h}_t | \mathbf{h}_h) \propto (\|\mathbf{h}_t\|^2 + \|\mathbf{h}_h\|^2)^{-N_{ht}/2} \quad (30)$$

$$= \|\mathbf{h}_h\|^{-N_{ht}} \left( 1 + \frac{\|\mathbf{h}_t\|^2}{\|\mathbf{h}_h\|^2} \right)^{-N_{ht}/2} \quad \text{for } \|\mathbf{h}_h\| \neq 0 \quad (31)$$

$$\propto p_{\text{St}}(\mathbf{h}_t; \nu, \Sigma) \quad \begin{matrix} \nu = N_h \\ \Sigma = \frac{\|\mathbf{h}_h\|^2}{N_h} I_{N_t} \end{matrix} \quad (32)$$

where  $p_{\text{St}}$  is the multivariate  $t$ -distribution, and  $I_{N_t}$  is the  $N_t \times N_t$  identity matrix. In our setting we can identify  $N_h = N - N_0$  as the dimensions of  $\mathcal{S}_X$ , and  $N_t$  as the number of test points. When taking the limit to infinitely many test points, the multivariate  $t$ -distribution becomes a  $t$ -process. The condition  $\|\mathbf{h}_h\| \neq 0$  translates to the condition that we need at least  $N \geq N_0 + 1$  datapoints that cannot be interpolated with a nullspace polynomial.

Regarding the simplicity of (29–32), we suggest to view the SI distribution as the natural extension of the  $t$ -distributions for  $\nu = 0$  degrees of freedom.

We should mention at this point that  $t$ -processes have been suggested for regression by Shah et al. [2014]. In their work the  $t$ -process is a prior, and the number of degrees of freedom  $\nu$  is a hyperparameter chosen by the user to steer

<sup>5</sup>the name “polyharmonic” refers to the multiple application of the Laplace operator in (18)

<sup>6</sup>because the SI process is isotropic in  $\mathcal{S}_X$  and the map from  $\mathcal{S}_X$  to the input space is linear

the heaviness of the distribution tails and hence the robustness of the fit. By contrast, we obtain the  $t$ -process as the posterior from a SIP prior, and  $\nu$  is not a free parameter but depends on the number of observed datapoints.

We want to point out that for a given test point  $\mathbf{x}_t$ , the posterior is a univariate  $t$ -distribution, which is identical<sup>7</sup> to the elementary result that the mean of datapoints with i.i.d. Gaussian error but unknown variance follows a  $t$ -distribution. This is a good plausibility check and shows that the complex setting of the SI process contains a well-known result as a special case.

### 3.5 Credible intervals

While the posterior process is isotropic in  $\mathcal{S}_X$ , its width in input space at a specific test point remains to be determined. For this aim we add the test point  $\mathbf{x}_t$  to the datapoints  $\mathbf{x}_n$  and consider the extended data-spanned space  $\mathcal{S}_{X, \mathbf{x}_t}$ . The situation is illustrated in Figure 5. The set of all functions that have the same fixed value  $y_t$  at the test point  $\mathbf{x}_t$  can be described by the maximum posterior interpolant plus a *test function* that we will determine now.

For simplicity we set  $y_t = f_{X, \mathbf{y}}(\mathbf{x}_t) + 1$ ; in this case the test function must (i) vanish at all datapoints, (ii) attain  $f_t(\mathbf{x}_t) = 1$  at the test point, and (iii) have minimal  $\eta$ -norm among all such functions. This is in essence just another interpolation task, so we can directly write down the solution in analogy to (26–28):

$$\mathbf{g} = [g_{\mathbf{x}_t}(\mathbf{x}_n)]_n \quad (33)$$

$$\mathbf{m} = [\mathbf{x}_t^\nu]_\nu \quad (34)$$

$$\begin{pmatrix} 0 & \mathbf{g}^T & \mathbf{m}^T \\ \mathbf{g} & G & M^T \\ \mathbf{m} & M & 0 \end{pmatrix} \begin{pmatrix} a_t \\ \mathbf{a} \\ \mathbf{c} \end{pmatrix} = \begin{pmatrix} 1 \\ \mathbf{0} \\ \mathbf{0} \end{pmatrix} \quad (35)$$

$$f_t(\mathbf{x}) = a_t g_{\mathbf{x}_t}(\mathbf{x}) + \sum_{n=1}^N a_n g_{\mathbf{x}_n}(\mathbf{x}) + \sum_{|\nu| < \lfloor \eta \rfloor} c_\nu \mathbf{x}^\nu \quad (36)$$

Now, the  $\eta$ -norm of the test function is the scaling factor between the posterior's width in the space of interpolants and its width at the test point  $\mathbf{x}_t$ . Therefore, the *pointwise posterior* for at least  $N \geq N_0 + 1$  datapoints is

$$p(y_t | \mathbf{x}_t, X, \mathbf{y}) = p_{\text{St}}(y_t; \nu, s(\mathbf{x}_t)) \quad (37)$$

$$\nu = N_h = N - N_0 \quad (38)$$

$$s(\mathbf{x}_t) = \frac{1}{\sqrt{\nu}} \frac{|f_{X, \mathbf{y}}|_\eta}{|f_t|_\eta} \quad (39)$$

$$\sigma(\mathbf{x}_t) = \frac{1}{\sqrt{\nu - 2}} \frac{|f_{X, \mathbf{y}}|_\eta}{|f_t|_\eta} \quad (40)$$

where  $s$  and  $\sigma$  are the  $t$ -distribution's scale parameter and standard deviation, resp.

This is the first time that we need to evaluate the  $\eta$ -norm. For polyharmonic splines of the form (28) we conjecture that the  $\eta$ -norm is given by

$$|f_{X, \mathbf{y}}|_\eta = C \cdot \mathbf{a}^T G \mathbf{a} \quad (41)$$

$$C = (-1)^{\lceil \eta \rceil} \frac{\Gamma(\eta + \frac{1}{2}) \pi^{\frac{D+1}{2}}}{\Gamma(\eta + \frac{D}{2}) \Gamma(2\eta + 1)} \quad (42)$$

For positive half-integer  $\eta$  we give a prove in Appendix 7.5, and numerical evidence suggests that this result is indeed valid for all positive non-integer  $\eta$ .

Finally, we illustrate the main results of this section by showing an exemplary interpolation solution in Fig. 6. The shown sample paths have been calculated by the expensive but simple procedure of alternately (i) drawing from the pointwise posterior ( $t$ -distribution) and (ii) recalculating the pointwise posterior including the new datapoint.

<sup>7</sup>except for the replacement of  $N$  by  $N_h$

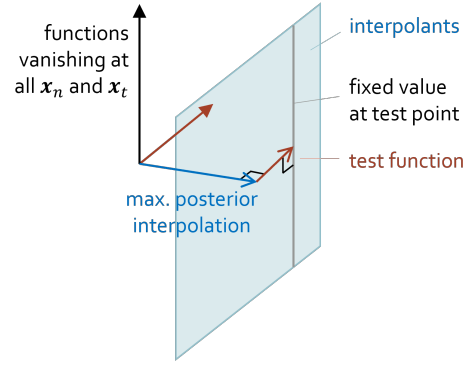


Figure 5: Test function to determine pointwise posterior



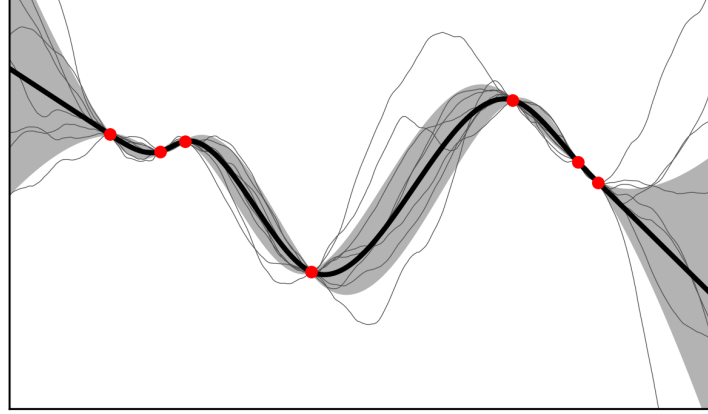


Figure 6: Interpolation of a few datapoints with the scale invariant process with  $\eta = 3/2$ . Shown is the maximum posterior estimate, pointwise standard deviation, and sample paths.

## 4 Regression

In this section, we formulate the posterior in  $\mathcal{S}_X^* = \mathcal{S}_X \times \mathcal{N}$  for a Gaussian likelihood, for which we first need to construct an orthonormal basis. An important finding is that the maximum posterior is a bad estimate because the posterior has a strong asymmetry. Therefore, we approximate the mean and covariance of the posterior with a sampling method.

To obtain the complete pointwise posterior (credible interval), we also consider the space of interpolants, which leads to the credible intervals having two different components, in contrast to Gaussian processes.

Finally, we consider the typical case where the size of the observation error (variance of data noise) is unknown.

### 4.1 Orthonormal basis

For the following we need an  $\eta$ -orthonormal basis of the data-spanned space  $\mathcal{S}_X$ . There are several ways to construct such a basis. Conceptually the simplest one (although not the most efficient) is an iterative procedure analogous to the test functions in Section 3.5.

We start with a minimal set of  $N_0 + 1$  datapoints  $X_{N_0+1} = [\mathbf{x}_1, \dots, \mathbf{x}_{N_0+1}]$  that span a single-dimensional subspace  $\mathcal{S}_{X_{N_0+1}}$  consisting only of multiples of  $f_{X_{N_0+1}}$ , see (23, 24). Then we consecutively add datapoints  $\mathbf{x}_{n+1}$ , each time constructing the corresponding “test function” (33–36) which is orthogonal to the previous space  $\mathcal{S}_{X_n}$ . The coefficients  $\mathbf{a}_{nm}$  of the initial spanning function and all test functions (leaving out the polynomial coefficients  $\mathbf{c}$ ) are collected in the matrix  $\tilde{H}$ :

$$\tilde{H} = \begin{pmatrix} a_{1,1} & a_{1,2} & \dots & a_{1,N_h-1} & a_{1,N_h} \\ \vdots & \vdots & & \vdots & \vdots \\ a_{N_0+1,1} & \vdots & & \vdots & \vdots \\ 0 & a_{N_0+2,2} & & \vdots & \vdots \\ \vdots & 0 & \ddots & \vdots & \vdots \\ \vdots & \vdots & & a_{N-1,N_h-1} & \vdots \\ 0 & 0 & \dots & 0 & a_{N,N_h} \end{pmatrix} \quad (43)$$

$N_h = N - N_0$  is the dimensionality of  $\mathcal{S}_X$ , and  $\tilde{H}$  is  $\eta$ -orthogonal by construction. After scaling all column vectors to unit  $\eta$ -norm by dividing by (41), we obtain the  $\eta$ -orthonormal  $H$ .

$$C \cdot H^T G H = I_{N_h} \quad (44)$$

where  $C$  is the constant (42) and  $I$  the identity matrix.

## 4.2 Prior in extended data-spanned space $\mathcal{S}_X^*$

As we did for interpolation in Section 3.2, we now need to consider the *extended* data-spanned space  $\mathcal{S}_x^* = \mathcal{S}_X \times \mathcal{N}$ . For the following we need the relation between the likelihood's mean  $\mu_y = \mathbf{y}$  and covariance  $\Sigma_y = \sigma_y I_N$  in output space ( $y$ -space), and its mean  $\mu_h$  and covariance  $\Sigma_h$  in  $\mathcal{S}_X^*$ . To get an overview, we give a diagram of the two steps involved.

$$\mathbf{h}^* = \begin{bmatrix} \mathbf{h} \\ \mathbf{c} \end{bmatrix} \xrightarrow{H} \begin{bmatrix} \mathbf{a} \\ \mathbf{c} \end{bmatrix} \xrightarrow{[B, M]} \mathbf{y} \quad (45)$$

The vectors  $\mathbf{h}^*$ ,  $\mathbf{a}$ , and  $\mathbf{y}$  have length  $N$ ,  $\mathbf{h}$  has length  $N_h$ , and  $\mathbf{c}$  has length  $N_0$ . We will use the superscript star  $*$  as a general notation to indicate that the nullspace is included:

$$\mathbf{a}^* = \begin{bmatrix} \mathbf{a} \\ \mathbf{c} \end{bmatrix} \quad H^* = \begin{bmatrix} H & 0 \\ 0 & I_{N_0} \end{bmatrix} \quad B^* = [B, M^T] \quad (46)$$

Now we can directly write down:

$$E^* = B^* H^* \quad (47)$$

$$\mathbf{y}_\mu = E^* \mathbf{h}_\mu^* \quad (48)$$

$$\Sigma_{h^*}^{-1} = (E^*)^T \Sigma_y^{-1} E^* \quad (49)$$

We obtain  $\mathbf{h}_\mu^*$  by solving (48) and  $\Sigma_{h^*}^{-1}$  by matrix multiplications (49). Now the likelihood in  $\mathcal{S}_X^*$  reads

$$p(\mathbf{y}|\mathbf{h}^*, X) \propto \exp\left(-\frac{1}{2}(\mathbf{h}^* - \mathbf{h}_\mu^*)^T \Sigma_{h^*}^{-1} (\mathbf{h}^* - \mathbf{h}_\mu^*)\right) \quad (50)$$

The prior over  $\mathbf{h}$  is scale invariant  $p_{\text{SI}}(\mathbf{h}) = \|\mathbf{h}\|^{-N_h}$ . Over the polynomial coefficients  $\mathbf{c}$  we choose a uniform prior. This is justified by the translation invariance of  $y$  and the linearity of the polynomials w.r.t. their coefficients. Together we have

$$p(\mathbf{h}^*) = \frac{1}{\|\mathbf{h}\|^{N_h}} \quad (51)$$

Note the difference between  $\mathbf{h}$  and  $\mathbf{h}^*$ . This prior over  $\mathbf{h}^*$  can be regarded as having a cylindrical symmetry.

## 4.3 Maximum posterior

The first idea to characterize the posterior is to find its maximum, because this is a good point estimate for most statistical problems. Setting the log posterior's gradient to zero gives ( $C^*$  denotes an undetermined constant)

$$\log p(\mathbf{h}^*|X, \mathbf{y}) = -N_h \log \|\mathbf{h}\| - \frac{1}{2}(\mathbf{h}^* - \mathbf{h}_\mu^*)^T \Sigma_{h^*}^{-1} (\mathbf{h}^* - \mathbf{h}_\mu^*) + C^* \quad (52)$$

$$\nabla \log p(\mathbf{h}^*|X, \mathbf{y}) = -N_h \frac{\mathbf{h}}{\|\mathbf{h}\|^2} - \Sigma_{h^*}^{-1} (\mathbf{h}^* - \mathbf{h}_\mu^*) = 0 \quad (53)$$

We can solve the resulting equation iteratively, starting at the interpolation solution  $\mathbf{h}_{(0)}^* = \mathbf{h}_\mu^*$ .

$$\left( \Sigma_{h^*}^{-1} + \frac{N_h}{\|\mathbf{h}_{(j-1)}\|^2} \begin{bmatrix} I_{N_h} & 0 \\ 0 & 0 \end{bmatrix} \right) \mathbf{h}_{(j)}^* = \Sigma_{h^*}^{-1} \mathbf{h}_\mu^* \quad (54)$$

This  $N \times N$  linear system must be solved for  $\mathbf{h}_{(j)}^*$  in each step.

Unfortunately, we found experimentally that the maximum posterior overregularizes significantly in most cases. The reason is that the hyperbolic prior grows fast towards the origin  $\|f\|_\eta = 0$ , while the volume near the origin is very small in high dimensions. Fig. 7 illustrates this situation. The trumpet-like shape of the grid illustrates the strong growth of volume as  $r$  increases. At its maximum, the posterior is very narrow in  $\phi$ -direction (where  $\phi$  comprises all  $N_0 - 1$  angles). As a result, the maximum posterior is significantly closer to the origin  $\|\mathbf{h}\| = 0$  than the bulk mass of the posterior (mean posterior).

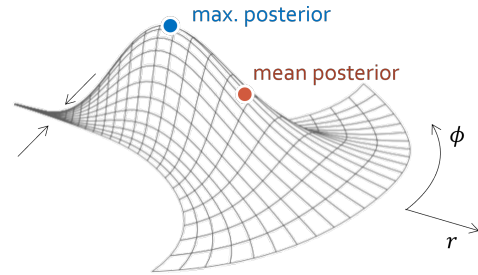


Figure 7: 2D illustration of the high-dimensional posterior in  $\mathcal{S}_X$ .

#### 4.4 Mean posterior and covariance

From this, it becomes clear that the maximum posterior is a bad point estimate, and instead we need the mean posterior. Unfortunately this involves an  $N$ -dimensional integral over  $\mathcal{S}_X^*$  that cannot be calculated directly. For now we will use a sampling method to find an approximation of the posterior’s mean and covariance. A more efficient method is possible and will be presented in a follow-up publication.

Our estimated posterior mean and covariance are the sample mean and sample covariance of the drawn samples  $\mathbf{h}_i^*$ :

$$\hat{\mathbf{h}}^* = \frac{1}{N_i} \sum_{i=1}^{N_i} \mathbf{h}_i^* \quad (55)$$

$$\hat{\Sigma}_{\mathbf{h}^*} = \frac{1}{N_i} \sum_{i=1}^{N_i} (\mathbf{h}_i^* - \hat{\mathbf{h}}^*)(\mathbf{h}_i^* - \hat{\mathbf{h}}^*)^T \quad (56)$$

#### 4.5 Nullspace pole

It is important to note that the prior’s pole at  $\|\mathbf{h}\| = 0$  does not get canceled by the likelihood<sup>8</sup>, and retains its infinite probability mass. This is in contrast to the typical situation where the Bayesian update turns improper priors into proper posteriors. Figure 8 illustrates the situation. Strictly speaking, this means that the posterior is confined to  $\|\mathbf{h}\| = 0$ , and SIP regression is reduced to polynomial regression within the nullspace.

The heuristic solution of this problem is obvious: We need to cut off the SI prior for  $|f|_\eta < c$ , where  $c$  should be near the saddle point’s  $\eta$ -norm. This works very well for all cases where the saddle point is pronounced. If there is no pronounced saddle point, we must consider the possibility that the true function  $f(\mathbf{x})$  is indeed a nullspace polynomial.

In practice we just check if the sampling procedure diverges to  $\|\mathbf{h}^*\| = 0$ .

If it does, SIP regression returns a polynomial; if it does not, it returns a regularized polyharmonic spline. Note that although this procedure is very simple, it constitutes an effective model selection technique that “automatically adapts to the data” in that the user is not required to fix the cutoff  $c$  or any other hyperparameter. It is an interesting topic for future work to clarify the relation between the “pronouncedness” of the saddle point and the probability that is attributed to nullspace polynomials by different model selection techniques.

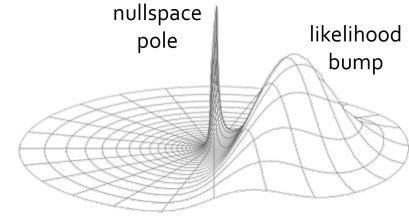


Figure 8: Sketch of posterior in  $\mathcal{S}_X$ .

#### 4.6 Unknown observation error

SIP regression can natively consider the full covariance of the observation error  $\Sigma_y$ , including non-identical and correlated errors. In most cases, however, it is reasonable to assume i. i. d. Gaussian errors with variance  $\sigma_y^2$

$$\Sigma_y = \sigma_y^2 I_N \quad (57)$$

However,  $\sigma_y^2$  is usually unknown. The standard approach is to treat  $\sigma_y$  as a hyperparameter and optimize it together with the model hyperparameters.

For SIP regression, however, our goal is to have as few hyperparameters as possible, so we would like to treat  $\sigma_y$  as a model parameter together with the coefficients of  $\mathbf{h}^*$ . For this, we need to choose a prior over  $\sigma_y$ , and since it is a scale parameter, we choose scale invariant “hyperbolic” prior

$$p(\sigma_y) \propto \frac{1}{\sigma_y} \quad (58)$$

Sampling from the combined parameters  $[\mathbf{h}^*, \sigma_y]$  with the corresponding distributions (52) and (58) is possible without problems.

Note that the SI prior over  $\sigma_y$  has the same issue as the SI process: The pole does not get canceled during inference, which means that strictly speaking the posterior assigns infinite probability mass to interpolation. We deal with this problem in the same way as before: If the saddle point is pronounced enough so that the sampling procedure does not find the nullspace pole, SIP regression effectively cuts off this “interpolation pole”; otherwise SIP regression reduces to interpolation.

<sup>8</sup>unless the error distribution  $p(y|f(\mathbf{x}))$  has finite support, i.e. vanishes for  $|y - f(\mathbf{x})| > C$  for some  $C$

#### 4.7 Posterior process and credible intervals

Up to now we have considered the regression posterior only in  $\mathcal{S}_X^*$ . To obtain the complete posterior process, we now include the orthogonal complement  $\mathcal{F}/\mathcal{S}_X^*$  into our consideration. By combining the posterior in  $\mathcal{S}_X^*$  with the  $t$ -process in  $\mathcal{F}/\mathcal{S}_X^*$ , we obtain an “ $N$ -dimensional mixture” of  $t$ -processes with different means  $f_{h^*}(\mathbf{x})$  and scale factors  $s_{h^*}(\mathbf{x})$

$$p(f|X, \mathbf{y}) = \int p_{\text{St}}(f; \nu, f_{h^*}, s_{h^*}) p(h^*|X, \mathbf{y}) dh^* \quad (59)$$

$$\nu = N_h \quad (60)$$

$$s_{h^*}(\mathbf{x}_t) = \frac{1}{\sqrt{\nu}} \frac{|f_{h^*}|_\eta}{|f_t|_\eta} \quad (61)$$

$$\sigma_{h^*}(\mathbf{x}_t) = \frac{1}{\sqrt{\nu-2}} \frac{|f_{h^*}|_\eta}{|f_t|_\eta} \quad (62)$$

For our current purposes it is sufficient to approximate (59) with a single  $t$ -process centered at the mean posterior  $f_{\hat{h}^*}$ . As approximate variance  $\sigma_f^2$  we use the squared sum of two terms  $\sigma_t^2$  and  $\sigma_s^2$  that represent the contributions of the  $t$ -process and the posterior covariance in  $\mathcal{S}_X^*$ , resp.

$$\sigma_f^2(\mathbf{x}) = \sigma_t^2(\mathbf{x}) + \sigma_s^2(\mathbf{x}) \quad (63)$$

$$\sigma_t(\mathbf{x}_t) = \sigma_{\hat{h}^*}(\mathbf{x}_t) \quad (64)$$

$$\frac{1}{\sigma_s^2(\mathbf{x}_t)} = \mathbf{x}_t^T (E^*)^{-T} \hat{\Sigma}_{h^*}^{-1} (E^*)^{-1} \mathbf{x}_t \quad (65)$$

$\sigma_t^2$  is the  $t$ -process’s variance at the mean posterior  $\hat{h}^*$ , and  $\sigma_s^2$  is the result of transforming the estimated covariance  $\hat{\Sigma}_{h^*}$  from  $\mathcal{S}_X^*$  back to input space. In the following we call  $\sigma_f$  the *function uncertainty*,  $\sigma_t$  the *interpolation uncertainty*, and  $\sigma_s$  the *spline uncertainty*.

Note that  $\sigma_f$  describes the uncertainty of our estimate of the true function  $f(\mathbf{x})$ , it does *not* contain the data noise. For very many datapoints,  $\sigma_f$  can become arbitrarily small, much smaller than the data noise. For some purposes (e.g. to assess the quality of the uncertainty estimates from held-out test points) it is necessary to add the data noise to the function uncertainty, to obtain the *data uncertainty*  $\sigma_d$

$$\sigma_d^2(\mathbf{x}) = \sigma_f^2(\mathbf{x}) + \sigma_y^2(\mathbf{x}) \quad (66)$$

Note that for Gaussian processes it is standard to report  $\sigma_d$  instead of  $\sigma_f$ .

## 5 Results

### 5.1 Details of sampling method

The following results are generated by sampling from the posterior in  $\mathcal{S}_X^*$  with the NUTS<sup>9</sup> sampler of pymc3 [Salvatier et al., 2016]. We used 2 chains with 1000 samples each, of which 500 are discarded as burn-in. As initial values we used the maximum posterior solution and (for the case of unknown data noise)  $\sigma_{y,\text{init}} = \sqrt{\text{Var}(\mathbf{y})}/10$ .

We found that sampling efficiency is quite bad with the standard parametrization of  $\mathcal{S}_X^*$  because different components of  $h^*$  are strongly correlated. Therefore, we first performed a reparametrization with the Cholesky decomposition of the covariance (Laplace approximation at the maximum posterior).

$$\hat{\Sigma}_{\text{Lapl}}^{-1} = LL^T \quad (67)$$

$$\tilde{h} = L^T h^* \quad (68)$$

To compare our results with Gaussian process regression, we use GPy [GPy, 2012], and always optimize all relevant hyperparameters.

### 5.2 First impression

A first impression of SIP regression is shown in Fig. 9 on a synthetic dataset with known data noise. It was generated by adding Gaussian noise of size  $\sigma_y = 0.08$  to the Higdon function [Gramacy and Lee, 2008]. The three SIP fits correspond to the true function assumed as continuous ( $\eta = 1/2$ ), once differentiable ( $\eta = 3/2$ ), and twice differentiable ( $\eta = 5/2$ ).

<sup>9</sup>Hamiltonian Monte Carlo with step-length chosen by the “No U-Turn” (NUTS) criterion

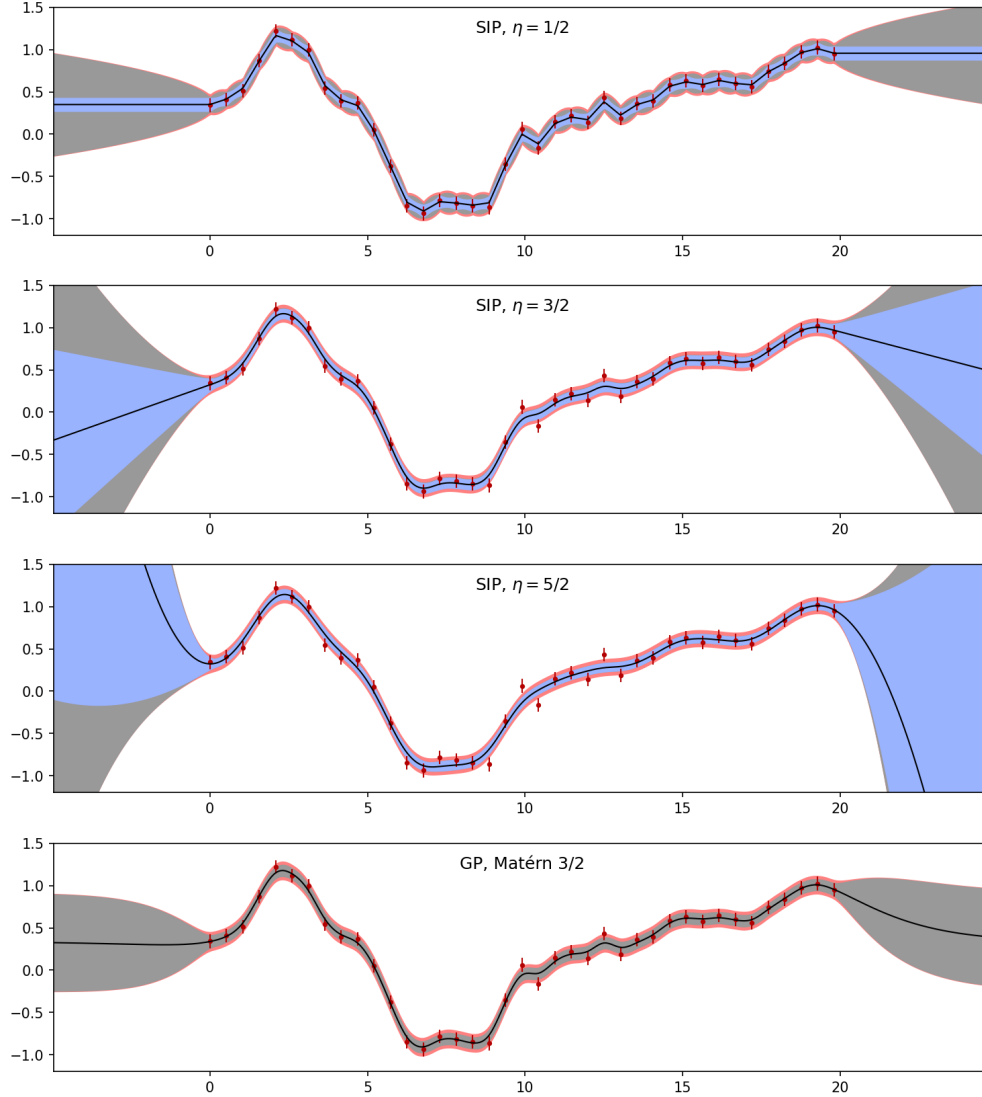


Figure 9: Fits of scale invariant process (SIP) and Gaussian process (GP) on a synthetic dataset with known data noise  $\sigma_y = 0.08$ . The three different credible intervals (blue, gray, red) are explained in the text.

Considering only the mean prediction (black line), the strength of regularization increases with the prescribed regularity  $\eta$ , as expected. SIP seems to regularize slightly stronger than the corresponding GP with a Matérn kernel of the same regularity ( $\eta = 3/2$ ).

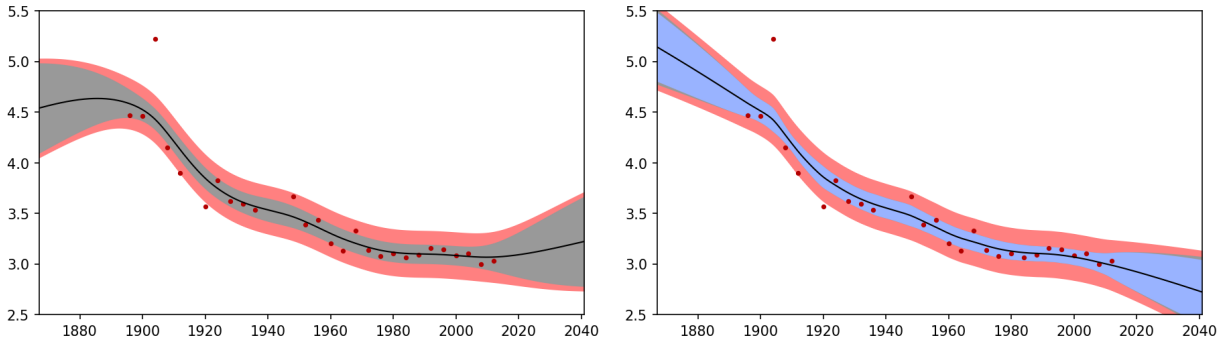
As explained in Section 4.7, SIP provides three different types of credible intervals. In Figures 9–11, the spline uncertainty  $\sigma_s(\mathbf{x})$  is shown blue, the function uncertainty  $\sigma_f$  (spline plus interpolation uncertainty) is gray, and data uncertainty  $\sigma_d$  (function unc. plus data noise) is red. In regions with abundant data, the interpolation uncertainty is very small (hardly visible in the plots). Note that the uncertainties are square-additive; therefore the red band has varying width although the data noise is constant. GPs do not have a separate spline uncertainty, therefore the complete interval of the function uncertainty is gray. Note that GPs report the complete data uncertainty by default, to obtain the function uncertainty one must specifically leave out the data noise.

### 5.3 Extrapolation behavior

In Figs. 9 and 10, the largest difference between SIP and GP is the extrapolation behavior. For SIP, the credible intervals increase quickly outside the data range, which correctly represents the lack of information in this region. For GPs, the credible intervals approach the “prior” mean and variance quite quickly. It is important to note that the “prior” mean

		marathon	diabetes	boston	energy eff. 0	energy eff. 1
# dims		1	10	13	8	8
# datapoints		27	442	506	768	768
kernel						
GP	Matérn 1/2	0.243	<b>54.32</b>	2.92	1.86	2.22
GP	Matérn 3/2	<b>0.219</b>	54.33	<b>2.83</b>	0.75	1.36
GP	Matérn 5/2	0.235	54.36	2.88	0.68	1.43
GP	rational quad.	0.234	64.91	2.91	<b>0.54</b>	<b>1.32</b>
GP	squared exp.	0.238	54.37	3.00	0.73	1.50
regularity						
SIP	$\eta = 1/2$	0.235	<b>54.23</b>	2.97	1.95	2.31
SIP	$\eta = 1.01$	<b>0.215</b>	54.60	<b>2.86</b>	1.10	1.62
SIP	$\eta = 3/2$	0.227	54.56	2.98	0.77	<b>1.36</b>
SIP	$\eta = 2.01$	0.556	54.50	3.38	0.70	1.51
SIP	$\eta = 5/2$	0.861	—	3.69	<b>0.62</b>	1.69

Table 1: Performance comparison on different datasets: RMSE of 5-fold cross-validation.

Figure 10: Best fits on marathon dataset. Left: GP, Matérn 3/2; right: SIP  $\eta = 1.01$ .

and variance are in fact hyperparameters that are optimized to the data. The name “prior” is hence quite inappropriate, it should rather be called “extrapolation mean” and “extrapolation variance”. The constant (and rather small) extrapolation variance of stationary GPs are obviously inappropriate, a fact that is often not pointed out.

One application where the credible intervals outside the data range are very important is Bayesian optimization, and we expect that SIP will have a significant advantage over GPs in this field.

#### 5.4 Real datasets

A performance comparison of SIP and GP on real datasets is shown in Table 1. For the multivariate datasets, all features were scaled to equal range (min-max), since automatic feature scaling (or automatic relevance determination ARD) is beyond the scope of this paper. For the datasets “boston” and “energy efficiency”, a small amount of jitter was added to the discrete features to avoid numerical problems.

The performance of the best variants of SIP and GP are very similar for all datasets. Also, there is a nice agreement concerning which variant is best for a given dataset; GP and SIP give similar “estimates” of the regularity of the true function.

The “marathon” dataset is univariate, so we can show the fits of the two best models in Fig. 10. It is interesting that the SIP shows the best result for the very low regularity of  $\eta = 1.01$ .

#### 5.5 Non-stationary data

Finally, we show fits of SIP and GP on a strongly non-stationary “step” dataset in Fig. 11. Neither SIP nor GP are really suitable for this kind of data, because they assume stationarity. However, alternative non-stationary methods are

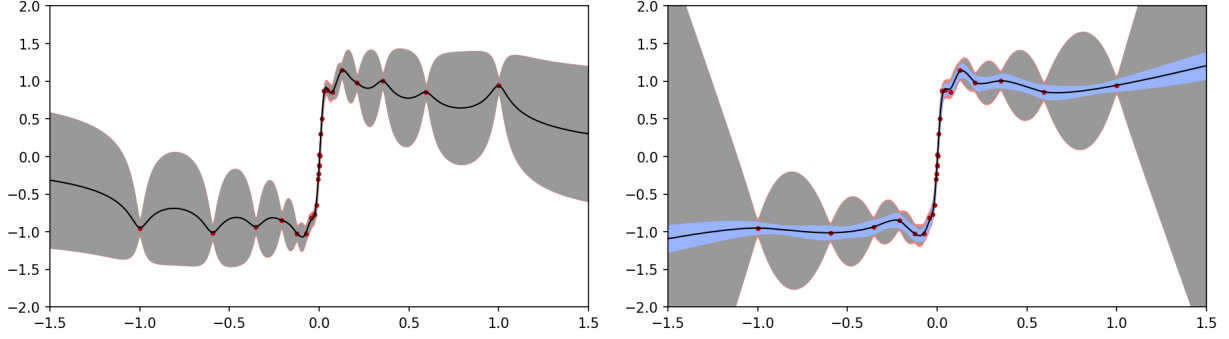


Figure 11: Best fits on non-stationary data. Left: GP, rational quadratic. Right: SIP,  $\eta = 1.01$

considerably more expensive and complex, so it is interesting how well standard GP and SIP work on non-stationary data.

Both methods have the problem that they learn a very small length scale to explain the step and hence strongly overfit in regions of scarce data. GPs have the additional problem that the predicted mean is biased towards the “prior” mean (or rather: extrapolation mean), which is obviously inappropriate.

## 6 Discussion

The main motivation to develop SIP regression was to derive an ML method from minimal assumptions. This has both theoretical and practical advantages. In the following we discuss the main points, although an exhaustive treatment of all consequences is beyond the scope of this paper.

### 6.1 Underlying assumptions

It is obvious that SIP has no kernel, no length scale, no variance (magnitude), and no prior mean. It is less obvious, however, which (possibly hidden) assumptions have been used in the derivation. Therefore, we give an overview and short discussion of all involved assumptions.

The most important assumption is the regularity  $\eta$  of the true function  $f(x)$ , a basic requirement for regularization. In applications, however, it is often unclear how  $\eta$  should be chosen. Therefore, we usually treat  $\eta$  as a hyperparameter that requires optimization for each dataset.

Another important assumption is the ellipsoidal symmetry we chose in Section 2.3. We believe that it is the simplest possible choice in the sense of maximum entropy, but since entropy is not well-defined for improper distributions, we cannot corroborate this claim.

All following assumptions can actually all be considered as being implied by the Euclidean structure of input and output space (i.e. Euclidean metric and Lebesgue volume measure), because Euclidean space is by definition translation and scale invariant. Still, it is helpful to point out how the different aspects of the Euclidean structure are used in SIP regression.

1. scale invariant output space ( $y$ -direction): hyperbolic SI process and hyperbolic error distribution (data noise)
2. scale invariant input space ( $x$ -direction): power-law spectrum
3. translation invariant output space: uniform prior over nullspace
4. translation invariant input space: stationary process
5. isotropic input space: no ARD

**1.** Both the hyperbolic SI process  $p(f)$  in (3) and the hyperbolic error distribution  $p(\sigma_y)$  in (58) have been derived from the scale invariance criterion in output space.

We want to stress that from an objective Bayesian viewpoint, a scale invariant prior is justified whenever there is no prior information about the true scale. It is not required to prove that the application really satisfies scale invariance. The true scale is learned from the data via the Bayesian update, and the posterior will exhibit this learned scale.

But of course there are limits to scale invariance, as we have seen in Section 4.5. Often there is a limited range of plausible scales. In some cases it is required to incorporate these limits into the prior to prevent wrong predictions (e.g. to cut off the nullspace and interpolation poles), but in most cases the scale information in the data is strong enough that putting these limits into the prior is not necessary.

2. Power-law spectra were chosen in Section 2.5 to achieve scale invariance in input space. It is a nice coincidence that this is equivalent to differential operators in position space. We want to stress, however, that there is actually no conceptual reason to use differential operators in statistics. We believe that the underlying reason why splines are successful is actually their scale invariance, *not* their connection to differential operators.

3. The uniform prior over nullspace is implied by translation invariance of output space, because the nullspace is parametrized by the polynomial coefficients  $\mathbf{c}$ , and the output  $f(x)$  depends linearly on  $\mathbf{c}$ .

4. Stationarity is implied by the translation invariance of Euclidean input space. It implies for instance that the posterior length scale of SIP regression is uniform over input space. For many applications, however, this assumption is not appropriate, because the features are not necessarily translation invariant. Therefore, stationarity is a serious restriction (see Section 6.4).

5. Isotropy of input space means in particular that the scale of different dimensions of input space (different features) are coupled. This assumption is appropriate only for few domains, e.g. geostatistics and spatial statistics. For all other applications, we should instead allow *independent* scaling of all features. Possible ways to mitigate or remove this assumption will be mentioned in Section 6.4.

## 6.2 Model assumptions vs. prior knowledge

We would like to stress that the assumptions in the above section are of a different type than most model assumptions in machine learning in that they are (i) very general, and (ii) can actually be considered as true.

When assuming, say, a Matérn kernel for Gaussian processes, we do not really believe that this kernel is “true”, but we just hope that the model can approximate the true correlations in the data well enough. Also, most applications do not provide a concrete indication of which kernel to choose, so the choice of kernel is usually rather arbitrary, and up to the personal experience, taste, and convenience of the ML practitioner. Actually we do not really “want” to choose a kernel in most cases, but we are forced to make a choice in order to apply GPs.

By contrast, consider the SIP assumptions of regularity  $\eta$  and Euclidean input and output space (in particular scale invariance). Regularity is a basic requirement to achieve generalization at all. Assuming Euclidean input and output space is also quite basic and general; while this assumption is not always appropriate (as discussed above), there are clear decision criteria for when it is and when it is not. In this sense, the assumptions of SIP regression can be considered as encoding a specific kind of prior knowledge, instead of being a (more or less) arbitrary or “constructed” model.

While this claim is quite strong, we should point out again the close relation between SIP regression and a hierarchical GP model based on a Wiener-type process. The conceptual advantages of SIP regression also apply to this hierarchical GP model, and hence we find it surprising that this topic has not been explored in the past.

## 6.3 Hyperparameter optimization

From a practical viewpoint, SIP regression has the important advantage of having only a single hyperparameter  $\eta$ . This promises a large potential speedup, because optimizing a single hyperparameter requires significantly fewer iterations than optimization in a high-dimensional space. This potential speed-up is not yet realized, because the employed sampling procedure is rather slow, but we will present a more efficient inference method for SIP regression in an upcoming publication.

## 6.4 Further work

The amount of possible follow-up work to the present paper is quite large. Here we just mention the most important open problems and possible extensions.

As mentioned before, the most pressing task for SIP regression is to find a more efficient inference method. The corresponding speed-up will in particular allow more experiments on larger datasets to test the performance of SIP regression more thoroughly.

The most severe methodical limitation of SIP regression is currently its restriction to isotropic input space. A straightforward remedy for this would be a built-in automatic feature scaling, similar to automatic relevance determination



(ARD) for GP regression. However, this approach has the disadvantage that the feature scales are hyperparameters that require optimization, which would negate one of the main advantages of SIP regression. To solve the problem fundamentally, an extension of the scale invariance principle to “feature-wise scale invariance” would be required.

The field where we expect SIP regression to have the largest practical impact is Bayesian optimization (BO). We have found in Section 5 that the extrapolation behavior of SIP regression is significantly better than for GP regression, especially, the credible intervals grow strongly outside the data range. Therefore, we expect that SIP-based BO will more easily find a good trade-off between exploration and exploitation.

## 7 Appendix

### 7.1 Marginal consistency of SI distributions

to be completed . . .

### 7.2 Regularity of scale invariant process

In this section, we show that the non-degenerate sample paths  $f(\mathbf{x})$  of the  $D$ -dimensional scale invariant process with amplitude spectrum  $a_\eta(\mathbf{k}) \propto \|\mathbf{k}\|^{-(\eta+D/2)}$  have regularity  $\eta$  almost surely.

The “degenerate” sample paths excluded above are the nullspace polynomials (which have zero  $\eta$ -norm) and all non-locally-bounded sample paths (which have infinite frequency amplitudes). Throughout our work, the term “regularity  $\eta$ ” is short for “[ $\eta$ ] times differentiable, with the [ $\eta$ ]-th derivative being locally Hölder continuous with exponent  $\alpha < \eta - [\eta]$ ”.

In the following we consider the sample paths over a bounded domain, for convenience chosen as the hypercube  $\|\mathbf{x} - \boldsymbol{\xi}\|_\infty \leq 1$ , where  $\mathbf{x}$  is the fixed center and  $\boldsymbol{\xi}$  the free variable. The corresponding domain in frequency space is the integer grid  $\mathbf{k} \in \mathbb{Z}^D$ , and the  $\eta$ -norm of the non-degenerate sample paths on the hypercube is finite almost surely.

$$|f|_{\eta, \mathbf{x}} = \sum_{\mathbf{k} \in \mathbb{Z}^D} \left| \frac{f(\mathbf{k})}{a_\eta(\mathbf{k})} \right|^2 < \infty \quad (69)$$

Note that  $f(\mathbf{x})$  is real and  $f(\mathbf{k})$  is complex with symmetry  $f(\mathbf{k}) = f^*(-\mathbf{k})$ .

The following proof uses two equivalent representations of the fractional Laplacian [Kwaśnicki, 2017]: as an integral in position space and as a Fourier transform. The Laplace exponent  $m$  must be positive and neither an integer nor a half-integer.

$$\Delta^m f(\mathbf{x}) \propto \int_{\|\mathbf{x} - \boldsymbol{\xi}\|_\infty < 1} \frac{f(\mathbf{x}) - f(\boldsymbol{\xi})}{\|\mathbf{x} - \boldsymbol{\xi}\|^{2m+D}} d\boldsymbol{\xi} \quad (70)$$

$$= \sum_{\mathbf{k} \in \mathbb{Z}^D} \|\mathbf{k}\|^{2m} \exp(i2\pi \mathbf{k} \mathbf{x}) f(\mathbf{k}) \quad (71)$$

We will relate the singular integral representation (70) to the Hölder condition, and the Fourier representation (71) to the spectrum, which together implies the equivalence between spectrum  $a_\eta$  and regularity  $\eta$ .

**Local Hölder continuity and fractional Laplacian** The regularity  $\eta$  (differentiability plus Hölder continuity of the derivative) can be described as:

$$|f(\mathbf{x}) - f(\boldsymbol{\xi})| \leq C \|\mathbf{x} - \boldsymbol{\xi}\|^\eta \quad \text{for } \|\mathbf{x} - \boldsymbol{\xi}\|_\infty < 1 \quad (72)$$

Inserting this into (70), we obtain

$$\Delta^m f(\mathbf{x}) \propto \int_{\|\mathbf{x} - \boldsymbol{\xi}\|_\infty < 1} \frac{f(\mathbf{x}) - f(\boldsymbol{\xi})}{\|\mathbf{x} - \boldsymbol{\xi}\|^{2m+D}} d\boldsymbol{\xi} \quad (73)$$

$$\leq \int_{\|\mathbf{x} - \boldsymbol{\xi}\|_\infty < 1} \frac{|f(\mathbf{x}) - f(\boldsymbol{\xi})|}{\|\mathbf{x} - \boldsymbol{\xi}\|^{2m+D}} d\boldsymbol{\xi} \quad (74)$$

$$\leq C \int_{\|\mathbf{x} - \boldsymbol{\xi}\|_\infty < 1} \frac{1}{\|\mathbf{x} - \boldsymbol{\xi}\|^{2m+D-\eta}} d\boldsymbol{\xi} \quad (75)$$

$$\leq \infty \quad \text{iff } 2m < \eta \quad (76)$$

i.e. the fractional Laplacian of order  $m$  is finite iff the  $f(\mathbf{x})$  is  $\eta$ -Hölder continuous and  $2m < \eta$ .

**Fractional Laplacian and frequency spectrum** The Fourier representation of the fractional Laplacian can be written as an inner product in the SI process's function space  $\mathcal{F}_\eta$ .

$$\Delta^m f(\mathbf{x}) = \sum_{\mathbf{k} \in \mathbb{Z}^D} \|\mathbf{k}\|^{2m} \exp(i2\pi \mathbf{k} \mathbf{x}) f(\mathbf{k}) \quad (77)$$

$$= \sum_{\mathbf{k} \in \mathbb{Z}^D} \frac{\|\mathbf{k}\|^{2m-2\eta-D}}{\|\mathbf{k}\|^{2\eta+D}} \exp(i2\pi \mathbf{k} \mathbf{x}) f(\mathbf{k}) \, d\mathbf{k} \quad (78)$$

$$= \left\langle \|\mathbf{k}\|^{2m-2\eta-D} \exp(i2\pi \mathbf{k} \mathbf{x}), f(\mathbf{k}) \right\rangle_\eta \quad (79)$$

As mentioned above,  $f$  has finite  $\eta$ -norm almost surely, and therefore (79) will be finite almost surely iff the functions  $L_{\mathbf{x}} = \|\mathbf{k}\|^{2m-2\eta-D} \exp(i2\pi \mathbf{k} \mathbf{x})$  have finite  $\eta$ -norm. This is the case iff

$$\left| L_{\mathbf{x}} \right|_\eta^2 = \left| \|\mathbf{k}\|^{2m-2\eta-D} \exp(i2\pi \mathbf{k} \mathbf{x}) \right|_\eta^2 < \infty \quad (80)$$

$$\sum_{\mathbf{k} \in \mathbb{Z}^D} \frac{\|\mathbf{k}\|^{2(2m-2\eta-D)}}{\|\mathbf{k}\|^{-(2\eta+D)}} \, d\mathbf{k} < \infty \quad (81)$$

$$4m - 2\eta - D < -D \quad (82)$$

$$2m < \eta \quad (83)$$

### 7.3 Nullspace polynomials

In this section, we show that polynomials of degree strictly smaller than  $\eta$  have zero  $\eta$ -norm. We perform the calculation in frequency space, where the monomials are represented as derivatives of the delta-function  $\delta(\mathbf{k})$ . With  $\mathbf{x} \in \mathbb{R}^D$  and a multi-index  $\boldsymbol{\nu} = [\nu_1, \dots, \nu_D]$ , we can write

$$f_{\boldsymbol{\nu}}(\mathbf{x}) = \mathbf{x}^{\boldsymbol{\nu}} = \prod_{d=1}^D x_d^{\nu_d} \quad (84)$$

$$f_{\boldsymbol{\nu}}(\mathbf{k}) = \partial^{\boldsymbol{\nu}} \delta(\mathbf{k}) = \prod_{d=1}^D \partial_d^{\nu_d} \delta(k_d) \quad (85)$$

The central idea of the proof is that the SI process's amplitude spectrum  $a_\eta(\mathbf{k}) = \|\mathbf{k}\|^{-(\eta+D/2)}$  has a zero at  $\mathbf{k} = 0$  which cancels delta-function derivatives up to a certain order.

For the calculation we treat the  $\delta$ -derivatives as the limit of a Gaussian function  $g(\mathbf{k})$  with infinitesimal width. For the scaling argument below it is convenient to separate the normalization factor  $s^D$  from the function shape  $g(\mathbf{k})$ .

$$g(\mathbf{k}) = \frac{1}{(2\pi)^{D/2}} \exp\left(-\frac{1}{2}\|\mathbf{k}\|^2\right) \quad (86)$$

$$\delta(\mathbf{k}) = \lim_{s \rightarrow \infty} s^D g(s\mathbf{k}) \quad (87)$$

$$\partial^{\boldsymbol{\nu}} \delta(\mathbf{k}) = \lim_{s \rightarrow \infty} s^D s^{|\boldsymbol{\nu}|} g^{(\boldsymbol{\nu})}(s\mathbf{k}) \quad (88)$$

where the factor of  $s^{|\boldsymbol{\nu}|}$  with  $|\boldsymbol{\nu}| = \sum_d \nu_d$  comes from the chain rule.

Now we can calculate the  $\eta$ -norm of  $f_\nu(\mathbf{k})$  by substituting  $\kappa = s\mathbf{k}$  in (91) below.

$$|f_\nu|_\eta^2 = \int_{\mathbb{R}^D} \left( \frac{f_\nu(\mathbf{k})}{a_\eta(\mathbf{k})} \right)^2 d\mathbf{k} \quad (89)$$

$$= \lim_{s \rightarrow \infty} \int_{\mathbb{R}^D} \left( \frac{s^{|\nu|+D} g^{(\nu)}(s\mathbf{k})}{\|\mathbf{k}\|^{-(\eta+\frac{D}{2})}} \right)^2 d\mathbf{k} \quad (90)$$

$$= \lim_{s \rightarrow \infty} \int_{\mathbb{R}^D} \frac{s^{2|\nu|+2D}}{s^{2\eta+D}} \left( \frac{g^{(\nu)}(\kappa)}{\|\kappa\|^{-(\eta+\frac{D}{2})}} \right)^2 \frac{1}{s^D} d\kappa \quad (91)$$

$$= \int_{\mathbb{R}^D} \left( \frac{g^{(\nu)}(\kappa)}{\|\kappa\|^{-(\eta+\frac{D}{2})}} \right)^2 d\kappa \cdot \lim_{s \rightarrow \infty} \frac{s^{2|\nu|}}{s^{2\eta}} \quad (92)$$

$$= \begin{cases} 0 & |\nu| < \eta \\ C_{\eta,\nu} & |\nu| = \eta \\ \infty & |\nu| > \eta \end{cases} \quad (93)$$

where we have abbreviated the finite integral in (92) with the symbol  $C_{\eta,\nu}$ .

## 7.4 Growth-rate constraints

In this section, we determine which polyharmonic splines have finite  $\eta$ -norm, i.e. we derive a constraint on the coefficients  $a_n$ . For readability we reprint the definitions of the polyharmonic spline  $f$  in position and frequency space. Since the polynomial term does not contribute to the  $\eta$ -norm, we leave it out.

$$f(\mathbf{x}) = \sum_{n=1}^N a_n \|\mathbf{x} - \mathbf{x}_n\|^{2\eta} \quad (94)$$

$$f(\mathbf{k}) = \sum_{n=1}^N a_n \frac{\exp(i2\pi \mathbf{k} \mathbf{x}_n)}{\|\mathbf{k}\|^{2\eta+D}} \quad (95)$$

We treat the problem in frequency space, where the  $\eta$ -norm of the polyharmonic spline  $f$  is defined as follows, and it is convenient to define the function  $h$ .

$$|f|_\eta = \int_{\mathbb{R}^D} \frac{f^2(\mathbf{k})}{\|\mathbf{k}\|^{-(2\eta+D)}} d\mathbf{k} \quad (96)$$

$$= \int_{\mathbb{R}^D} \frac{h^2(\mathbf{k})}{\|\mathbf{k}\|^{2\eta+D}} d\mathbf{k} \quad (97)$$

$$h(\mathbf{k}) = \|\mathbf{k}\|^{2\eta+D} \cdot f(\mathbf{k}) = \sum_{n=1}^N a_n \exp(i2\pi \mathbf{k} \mathbf{x}_n) \quad (98)$$

To understand for which coefficients  $\mathbf{a}$  the norm  $|f|_\eta$  is finite, first note that  $h^2(\mathbf{k})$  alternates symmetrically around 0, and hence the integral (97) converges for  $\mathbf{k} \rightarrow \infty$  for all  $2\eta + D > 0$ , which includes the complete domain of interest  $\eta > 0$ . The more complicated part is the convergence at the origin  $\mathbf{k} \rightarrow 0$ . Roughly speaking, since the denominator has a zero of degree  $2\eta + D$ , the numerator must have a zero of degree at least  $2\eta$  to achieve convergence. We will make this precise below.

To find coefficients  $\mathbf{a}$  such that  $h^2(\mathbf{k})$  has a zero of a degree  $2\eta$ , we consider the Taylor expansions of  $h(\mathbf{k})$  and  $h^2(\mathbf{k})$ .

$$h(\mathbf{k}) = \sum_{\nu} \alpha_{\nu} \mathbf{k}^{\nu} \quad \alpha_{\nu} = \frac{\partial^{\nu} h(\mathbf{k})}{\nu!} \quad (99)$$

$$h^2(\mathbf{k}) = \sum_{\nu} \beta_{\nu} \mathbf{k}^{\nu} \quad \beta_{\nu} = \sum_{|\tilde{\nu}| \leq |\nu|} \alpha_{\tilde{\nu}} \alpha_{\nu - \tilde{\nu}} \quad (100)$$

where  $\nu$  and  $\tilde{\nu}$  are a multi-indices,  $\nu! = \prod_d \nu_d!$ , and  $|\nu| = \sum_d \nu_d$ . Note that the Taylor coefficients  $\beta_{\nu}$  vanish up to degree  $2\eta$  if and only if  $\alpha_{\nu}$  vanish up to degree  $\eta$ ,

$$\beta_{\nu} = 0 \quad \forall |\nu| \leq 2\eta \quad (101)$$

$$\iff \alpha_{\nu} = 0 \quad \forall |\nu| \leq \eta \quad (102)$$

and the condition (102) can be written in terms of  $\mathbf{a}$  as

$$\alpha_{\boldsymbol{\nu}} = \frac{\partial^{\boldsymbol{\nu}} h(\mathbf{k})}{\boldsymbol{\nu}!} = \frac{2\pi i h(\mathbf{k})}{\boldsymbol{\nu}!} \cdot \sum_n a_n \mathbf{x}_n^{\boldsymbol{\nu}} = 0 \quad \forall |\boldsymbol{\nu}| < \eta \quad (103)$$

$$\sum_n a_n \mathbf{x}_n^{\boldsymbol{\nu}} = 0 \quad \forall |\boldsymbol{\nu}| < \eta \quad (104)$$

which is our sought result.

**Convergence of high-order Taylor terms** We have stated above “roughly speaking” that the integral (97)  $\int \mathbf{k}^{\boldsymbol{\nu}} / \|\mathbf{k}\|^{2\eta+D} d\mathbf{k}$  converges for  $|\boldsymbol{\nu}| > 2\eta$ . Now we provide a detailed proof for this. The idea is to divide the  $D$ -dimensional integral into an integral over zero-centered hyperspheres and an integral over the radius (or scale)  $s$ . Since  $\mathbf{k}^{\boldsymbol{\nu}}$  scales with  $s^{|\boldsymbol{\nu}|}$ , the hypersphere integral of  $\mathbf{k}^{\boldsymbol{\nu}}$  scales with  $s^{|\boldsymbol{\nu}|+D-1}$ .

$$(s\mathbf{k})^{\boldsymbol{\nu}} = s^{|\boldsymbol{\nu}|} \mathbf{k}^{\boldsymbol{\nu}} \quad (105)$$

$$q_{\boldsymbol{\nu}}(s) = \int_{\|\mathbf{k}\|=s} \mathbf{k}^{\boldsymbol{\nu}} d\mathbf{k} = s^{|\boldsymbol{\nu}|+D-1} q_{\boldsymbol{\nu}}(1) \quad (106)$$

Hence the integral of interest can be expressed as:

$$\int_{\|\mathbf{k}\| \leq 1} \frac{\mathbf{k}^{\boldsymbol{\nu}}}{\|\mathbf{k}\|^{2\eta+D}} d\mathbf{k} = q_{\boldsymbol{\nu}}(1) \int_0^1 \frac{s^{|\boldsymbol{\nu}|+D-1}}{s^{2\eta+D}} ds \quad (107)$$

$$= \begin{cases} \infty & |\boldsymbol{\nu}| \leq 2\eta \\ \frac{q_{\boldsymbol{\nu}}(1)}{|\boldsymbol{\nu}| - 2\eta} & |\boldsymbol{\nu}| > 2\eta \end{cases} \quad (108)$$

## 7.5 Inner product of polyharmonic splines

to be completed ...

## References

- Carl Edward Rasmussen and Christopher K. I. Williams. *Gaussian Processes for Machine Learning*. The MIT Press, 2005. ISBN 978-0-262-25683-4. doi:10.7551/mitpress/3206.001.0001. URL <https://direct.mit.edu/books/book/2320/gaussian-processes-for-machine-learning>.
- Seth Flaxman, Andrew Gelman, Daniel B. Neill, Alex Smola, and Aki Vehtari. Fast hierarchical Gaussian processes. 2015.
- George S. Kimeldorf and Grace Wahba. A Correspondence Between Bayesian Estimation on Stochastic Processes and Smoothing by Splines. *The Annals of Mathematical Statistics*, 41(2):495–502, 1970. ISSN 00034851. URL <http://www.jstor.org/stable/2239347>. Publisher: Institute of Mathematical Statistics.
- Jean Duchon. Splines minimizing rotation-invariant semi-norms in Sobolev spaces. In A. Dold, B. Eckmann, Walter Schempp, and Karl Zeller, editors, *Constructive Theory of Functions of Several Variables*, volume 571, pages 85–100. Springer Berlin Heidelberg, Berlin, Heidelberg, 1977. ISBN 978-3-540-08069-5 978-3-540-37496-1. doi:10.1007/BFb0086566. URL <http://link.springer.com/10.1007/BFb0086566>. Series Title: Lecture Notes in Mathematics.
- Grace Wahba. *Spline Models for Observational Data*. Society for Industrial and Applied Mathematics, January 1990. ISBN 978-0-89871-244-5 978-1-61197-012-8. doi:10.1137/1.9781611970128. URL <http://epubs.siam.org/doi/book/10.1137/1.9781611970128>.
- H. Wendland. *Scattered Data Approximation*. Cambridge Monographs on Applied and Computational Mathematics. Cambridge University Press, 2004. ISBN 978-1-139-45665-4. URL <https://books.google.de/books?id=qy4cbWUmSyYC>.
- G.E. Fasshauer. *Meshfree Approximation Methods with MATLAB*. Interdisciplinary mathematical sciences. World Scientific, 2007. ISBN 978-981-270-633-1. URL <https://books.google.de/books?id=gtqBdMEqyEC>.
- Dirk P. Kroese and Zdravko I. Botev. Spatial Process Simulation. In Volker Schmidt, editor, *Stochastic Geometry, Spatial Statistics and Random Fields*, volume 2120, pages 369–404. Springer International Publishing, Cham, 2015. ISBN 978-3-319-10063-0 978-3-319-10064-7. doi:10.1007/978-3-319-10064-7\_12. URL [http://link.springer.com/10.1007/978-3-319-10064-7\\_12](http://link.springer.com/10.1007/978-3-319-10064-7_12). Series Title: Lecture Notes in Mathematics.

- Encyclopedia. Wiener field, 2020. URL [http://encyclopediaofmath.org/index.php?title=Wiener\\_field&oldid=50607](http://encyclopediaofmath.org/index.php?title=Wiener_field&oldid=50607).
- J. T. Kent and K. V. Mardia. The link between kriging and thin-plate splines. In F. P. Kelly, editor, *Probability, statistics and optimization : a tribute to Peter Whittle*, pages 325–339. Wiley, 1994.
- Encyclopedia. Hurst, Harold Edwin, 2016. URL [http://encyclopediaofmath.org/index.php?title=Hurst,\\_Harold\\_Edwin&oldid=39213](http://encyclopediaofmath.org/index.php?title=Hurst,_Harold_Edwin&oldid=39213).
- Patrick Flandrin. On the Spectrum of Fractional Brownian Motions. *IEEE Transactions on Information Theory*, 35(1): 197–199, January 1989.
- G. M. Molchan. Some problems for Lévy’s Brownian motion. 12:682–690, 1967.
- I. M. Gelfand and G. E. Shilov. *Generalized functions, Volume 1*. American Mathematical Society : AMS Chelsea Publishing, Providence, Rhode Island, 2016 edition edition, 1964. ISBN 978-1-4704-2658-3 978-1-4704-3122-8. URL <https://bookstore.ams.org/chel-377-h/>.
- Amar Shah, Andrew Wilson, and Zoubin Ghahramani. Student-t Processes as Alternatives to Gaussian Processes. In Samuel Kaski and Jukka Corander, editors, *Proceedings of the Seventeenth International Conference on Artificial Intelligence and Statistics*, volume 33 of *Proceedings of Machine Learning Research*, pages 877–885, Reykjavik, Iceland, April 2014. PMLR. URL <https://proceedings.mlr.press/v33/shah14.html>.
- John Salvatier, Thomas V. Wiecki, and Christopher Fonnesbeck. Probabilistic programming in Python using PyMC3. *PeerJ Computer Science*, 2:e55, April 2016. ISSN 2376-5992. doi:10.7717/peerj-cs.55. URL <https://peerj.com/articles/cs-55>.
- GPy. GPy: A Gaussian process framework in python, 2012. URL <http://github.com/SheffieldML/GPy>.
- Robert B Gramacy and Herbert K. H Lee. Bayesian Treed Gaussian Process Models With an Application to Computer Modeling. *Journal of the American Statistical Association*, 103(483):1119–1130, September 2008. ISSN 0162-1459, 1537-274X. doi:10.1198/016214508000000689. URL <https://www.tandfonline.com/doi/full/10.1198/016214508000000689>.
- Mateusz Kwaśnicki. Ten Equivalent Definitions of the Fractional Laplace Operator. *Fractional Calculus and Applied Analysis*, 20(1):7–51, February 2017. ISSN 1311-0454, 1314-2224. doi:10.1515/fca-2017-0002. URL <https://link.springer.com/10.1515/fca-2017-0002>.